Bound states of dipolar molecules studied with the Berggren expansion method

K. Fossez, N. Michel, W. Nazarewicz, and M. Płoszajczak

Bound states of dipolar molecules studied with the Berggren expansion method

K. Fossez,[1] N. Michel,[2,3] W. Nazarewicz,[2,3,4] and M. Płoszajczak[5]

[1]Grand Accélérateur National d'Ions Lourds (GANIL),
CEA/DSM - CNRS/IN2P3, BP 55027, F-14076 Caen Cedex, France
[2]Department of Physics & Astronomy, University of Tennessee, Knoxville, Tennessee 37996, USA
[3]Physics Division, Oak Ridge National Laboratory, Oak Ridge, Tennessee 37831, USA
[4]Institute of Theoretical Physics, University of Warsaw, ul. Hoża 69, 00-681 Warsaw, Poland
[5]Grand Accélérateur National d'Ions Lourds (GANIL),
CEA/DSM - CNRS/IN2P3, BP 55027, F-14076 Caen Cedex, France
(Dated: April 12, 2013)

Bound states of dipole-bound anions are studied by using a non-adiabatic pseudopotential method and the Berggren expansion involving bound states, decaying resonant states, and non-resonant scattering continuum. The method is benchmarked by using the traditional technique of direct integration of coupled channel equations. A good agreement between the two methods has been found for well-bound states. For weakly-bound subthreshold states with binding energies comparable with rotational energies of the anion, the direct integration approach breaks down and the Berggren expansion method becomes the tool of choice.

I. INTRODUCTION

Weakly-bound systems are intensely studied in different domains of mesoscopic physics [1, 2], including nuclear [3–7], molecular [8–15], and atomic [16–18] physics. In this context, dipolar anions are one of the most spectacular examples of marginally bound quantum systems [19–40].

The mechanism for forming anion states by the long-range dipolar potential has been proposed by Fermi and Teller [41], who studied the capture of negatively charged mesons in matter. They found that if a negative meson is captured by a hydrogen nucleus, the binding energy of the electron becomes zero for the electric dipole moment of a meson-proton system $\mu_{cr} = 1.625$ D. Later this result was generalized to the case of an extended dipole with an infinite moment of inertia [42]. Lifting the adiabatic approximation by considering the rotational degrees of freedom of the anion [19–24] turned out to be crucial; it also boosted the critical value of μ to about 2.5 D. For anions with $\mu > \mu_{cr}$, the number of bound states of the electron becomes finite, and the critical electric dipole moment μ_{cr} depends on the moment of inertia of the molecule. In the non-adiabatic calculations, the pseudo-potential was used to take into account finite size effects, repulsive core, polarization effects, and quadrupolar interaction. The pseudo-potential method has provided a convenient description of binding energy of the electron bound by an electric dipolar field. Recently, this method was applied to linear electric quadrupole systems [43]. Some recent theoretical studies of dipole-bound anions also employed the coupled cluster technique [44–46].

The unbound part of the spectrum of multipolar anions has been discussed theoretically in Refs. [47, 48] and Refs. quoted therein. Resonance energies of dipolar anions have been determined experimentally by low energy electron scattering off the dipolar molecules [27, 28, 31, 33, 35].

Both the long-range dipole potential and the weak binding of dipolar anions provide a considerable challenge for theory. The impact of the molecular rotation on a weakly-bound electron can be represented by coupled-channel (CC) equations that can be solved by means of the direct integration. While this approach correctly predicts the number of bound states of polar anions, it is less precise for treatment of weakly-bound excited states. Moreover, it cannot be used for studies of dipolar anion resonances because the exact asymptotics for a dipolar potential in the presence of a molecular rotor cannot be determined.

In this paper, we apply the complex-energy configuration interaction framework based on the Berggren ensemble [49] to the problem of bound states in dipole-bound anions. The Berggren completeness relation is a resonant-state expansion; it treats the resonant and scattering states on the same footing as bound states. We have successfully applied this tool to a variety of nuclear structure problems pertaining to weakly-bound and unbound nuclear states [50–53] (for a recent review see Ref. [54]). The nuclear many-body realisation of the complex energy configuration interaction method is known under the name of the Gamow Shell Model.

Resonances do not belong to the Hilbert space, so the mathematical apparatus of quantum mechanics in Hilbert space is inadequate for Gamow states [55], which are not square-integrable. It turned out that the mathematical structure of the Rigged Hilbert Space (RHS) [56–58] can accommodate time-asymmetric processes, such as particle decays, by extending the domain of quantum mechanics. The mathematical setting of the resonant state expansions follows directly from the formulation of quantum mechanics in the RHS [56, 57], rather than the usual Hilbert space [58–60].

The Berggren ensemble provides a natural generaliza-

tion of the configuration interaction for the description of the particle continuum. The complex-energy Gamow-Siegert states [55, 61] states have been used in various contexts in nuclear, atomic, and molecular physics [62–75]. Some recent applications of Gamow-Siegert states, also in the context of a CC formalism relevant to the problem of dipole anions, can be found in, e.g., Refs. [76–80].

This paper is organized as follows. The Hamiltonian of the pseudo-potential method is briefly discussed in Sec. II. The CC formulation of the Schrödinger equation for dipole-bound anions is outlined in Sec. III. Section IV discusses the direct integration method (DIM) for solving the CC problem with a focus on difficulties in imposing proper boundary conditions when the rotational motion of the molecule is considered. The Bergggren expansion method (BEM) is introduced in Sec. V. Section VI specifies the coupling constants of the pseudo-potential and other calculation parameters. Salient features of DIM and BEM solutions are compared in Sec. VII. The predictions of DIM and BEM for low-lying energy states and r.m.s. radii of LiI$^-$, LiCl$^-$, LiF$^-$, and LiH$^-$ anions are collected in Sec. VIII. Finally, Sec. IX contains the conclusions and outlook.

II. HAMILTONIAN

A dipole-bound anion is composed of a neutral polar molecule with a dipole moment greater than μ_{cr} and a valence electron. The Hamiltonian of the total system can be written as:

$$H_{tot} = H_e + H_{mol} + V \tag{1}$$

where H_e is the Hamiltonian of the valence electron, H_{mol} is the Hamiltonian of the molecule, and V is the electron-molecule interaction. The many-body Schrödinger equation for H_{tot} couples all electrons of the system; hence, an approximation scheme has to be developed.

As a first simplification, we notice that since the vibrational motion of a molecule and core electron motions are much faster than both the rotational motion of a molecule and the orbital motion of a valence electron, the effective separation of slow motions from the fast is present in the system largely simplifying the dynamical equations [81]. Furthermore, the Hamiltonian (1) simplifies considerably if one considers anions of closed-shell systems. Moreover, if spin is neglected [24], the molecule can be treated as a rigid rotor. Note that the energy scales associated with the rotational motion of the molecule and the motion of the weakly-bound valence electron may be comparable. Consequently, there appears a strong non-adiabatic coupling between the molecular angular momentum $\boldsymbol{j}$ and the orbital angular momentum $\boldsymbol{\ell}$ of the electron. Eq. (1) thus writes within this approximation scheme:

$$H_{tot} = \frac{\boldsymbol{p}_e^2}{2m_e} + \frac{\boldsymbol{j}^2}{2I} + V \tag{2}$$

where I is the moment of inertia of the neutral molecule, $\boldsymbol{p}_e$ is the linear momentum of the valence electron and m_e its mass. The interaction V is approximated by a one-body pseudo-potential $V(r, \theta)$ acting on the valence electron [24, 82, 83]:

$$V(r,\theta) = V_\mu(r,\theta) + V_\alpha(r,\theta) + V_{Q_{zz}}(r,\theta) + V_{\text{SR}}(r), \tag{3}$$

where θ is the angle between the dipolar charge separation $\boldsymbol{s}$ and electron coordinate;

$$V_\mu(r,\theta) = -\mu e \sum_{\lambda=1,3,\cdots} \left(\frac{r_<}{r_>}\right)^\lambda \frac{1}{sr_>} P_\lambda(\cos\theta) \tag{4}$$

is the dipole potential of the molecule;

$$V_\alpha(r,\theta) = -\frac{e^2}{2r^4}\left[\alpha_0 + \alpha_2 P_2(\cos\theta)\right] f(r) \tag{5}$$

is the induced dipole potential, where α_0 and α_2 are the spherical and quadrupole polarizabilities of the linear molecule;

$$V_{Q_{zz}}(r,\theta) = -\frac{e}{r^3} Q_{zz} P_2(\cos\theta) f(r) \tag{6}$$

is the potential due to the permanent quadrupole moment of the molecule; and a short-range potential

$$V_{\text{SR}}(r) = V_0 \exp(-(r/r_c)^6), \tag{7}$$

where r_c is a range radius, which accounts for the exchange effects and compensates for spurious effects induced by the cut-off function

$$f(r) = 1 - \exp\{-(r/r_0)^6\} \tag{8}$$

introduced in Eqs. (5,6) to avoid a singularity at $r \to 0$. The parameter r_0 in Eq. (8) is an effective short-range cutoff distance for the long-range interactions.

III. COUPLED-CHANNEL EXPRESSION OF THE HAMILTONIAN

The eigenfunctions of the Hamiltonian (2) can be conveniently expressed in the CC representation:

$$\Psi^J = \sum_c u_c^J(r) \Phi_{j_c\ell_c}^J \tag{9}$$

where the index c labels the channel, $u_c^J(r)$ is the radial wave function of the valence electron in a channel c, and the channel function $\Phi_{j_c\ell_c}^J$ arises from the coupling of j_c and ℓ_c to the total angular momentum J of the anion: $\boldsymbol{j} + \boldsymbol{\ell} = \boldsymbol{J}$. Due to rotational invariance of H_{tot}, its matrix elements are independent of the magnetic quantum number M, which will be omitted in the following.

The potential $V(r,\theta)$ in Eqs. (3 - 7) can be expanded in multipoles:

$$V(r,\theta) = \sum_\lambda V_\lambda(r) P_\lambda(\cos\theta), \tag{10}$$

where

$$P_\lambda(\cos\theta) = \frac{4\pi}{2\lambda+1} Y_\lambda^{(mol)}(\hat{s}) \cdot Y_\lambda^{(e)}(\hat{r}). \qquad (11)$$

The matrix elements of $P_\lambda(\cos\theta)$ between the channels c and c' are obtained by means of the standard angular momentum algebra:

$$\langle \Phi_{j_{c'}\ell_{c'}}^J | P_\lambda(\cos\theta) | \Phi_{j_c\ell_c}^J \rangle$$
$$= (-1)^{j_{c'}+j_c+J} \begin{Bmatrix} j_{c'} & \ell_{c'} & J \\ \ell_c & j_c & \lambda \end{Bmatrix} \begin{pmatrix} j_{c'} & \lambda & j_c \\ 0 & 0 & 0 \end{pmatrix} \begin{pmatrix} \ell_{c'} & \lambda & \ell_c \\ 0 & 0 & 0 \end{pmatrix}$$
$$\times \sqrt{(2\ell_{c'}+1)(2\ell_c+1)(2j_{c'}+1)(2j_c+1)}. \qquad (12)$$

In the following, we express r in units of the Bohr radius a_0, I in units of $m_e a_0^2$, and energy in Ry. The radial functions $u_c^J(r)$ are solutions of the set of CC equations:

$$\left[\frac{d^2}{dr^2} - \frac{\ell_c(\ell_c+1)}{r^2} - \frac{j_c(j_c+1)}{I} + E_J \right] u_c^J(r)$$
$$= \sum_{c'} v_{cc'}^J(r) u_{c'}^J(r), \qquad (13)$$

where E_J is the energy of the system and

$$v_{cc'}^J(r) = \sum_\lambda \langle \Phi_{j_{c'}\ell_{c'}}^J | P_\lambda(\cos\theta) | \Phi_{j_c\ell_c}^J \rangle V_\lambda(r). \qquad (14)$$

IV. DIRECT INTEGRATION OF COUPLED-CHANNEL EQUATIONS

The CC equations (13) can be solved by the DI method. Below we describe the method used to generate the channel wave functions $u_c(r)$ (from now on, the quantum number J is omitted to simplify notation) obeying the physical boundary conditions. Namely, we assume that $u_c(r)$ is regular at origin: $u_c(r=0)=0$, and for $r \to +\infty$ it behaves like an outgoing wave $u_c^+(r)$.

The central issue of DI lies in the boundary condition at infinity. Indeed, as we shall see in Sec. (IV B), an asymptotic wave function of a dipole-bound anion is not analytic in general, so that one cannot exactly impose outgoing boundary conditions. This calls for the use of controlled approximations. In the following, we describe the numerical integration of CC equations. While the method is standard (cf. Sec. 3.3.2 of Ref. [84]), this particular application is not; hence key details should be given.

A. The basis method with the direct integration

To integrate CC equations, we introduce the matching radius r_m that defines the internal region $[0:r_m]$, where the centrifugal potential is appreciable, and the external zone $[r_m : +\infty]$. An internal basis function $u_{b;c}^0(r)$ in $[0:r_m]$ is regular at $r=0$:

$$u_{b;c_b}^0(r) \sim r^{\ell_{c_b}+1} \qquad (15)$$

in one channel $c_b = (j_{c_b}, \ell_{c_b})$ and $u_{b;c}^0(r) = o(r^{\ell_{c_b}+1})$ for $c \neq c_b$, which form the fundamental boundary conditions of the CC equations for $r \to 0$. In order to find an equivalent of $u_{b;c}^0(r)$ in this case, we write the CC equations (13) at zeroth order in $u_b^0;c(r)$:

$$[u_{b;c}^0]''(r) = \frac{\ell_c(\ell_c+1)}{r^2} u_{b;c}^0(r)$$
$$+ \left(v_{cc}^J(0) + \frac{j_c(j_c+1)}{I} - E_J \right) u_{b;c}^0(r)$$
$$+ \sum_{c' \neq c} v_{cc'}^J(0) u_{c'}(r) + O(u_{b;c}^0(r)). \qquad (16)$$

Due to the fundamental boundary conditions of CC equations at $r \to 0$, the second term on the right-hand side of (16) and all terms in the sum for which $c' \neq c_b$ are $O(r^{\ell_{c_b}+1})$, and $u_{b;c_b}^0 = r^{\ell_{c_b}+1}$. Thus, Eq. (16) becomes:

$$[u_{b;c}^0]''(r) = \frac{\ell_c(\ell_c+1)}{r^2} u_{b;c}^0(r) + v_{cc_b}^J(0) r^{\ell_{c_b}+1}$$
$$+ O(r^{\ell_{c_b}+1}). \qquad (17)$$

Equation (17) can be integrated analytically along with the fundamental boundary conditions of CC equations for $r \to 0$ if one neglects the rest term equal to $o(r^{\ell_{c_b}+1})$. The internal channel wave functions $u_{b;c}^0(r)$ with $c \neq c_b$ and $r \to 0$ thus read:

$$v_{cc_b}^J(0) \times \begin{cases} \dfrac{r^{\ell_{c_b}+3}}{2\ell_{c_b}+5} \ln(r/r_m) & \text{for } \ell_c = \ell_{c_b}+2, \\[2ex] \dfrac{r^{\ell_{c_b}+3}}{(\ell_{c_b}+2)(\ell_{c_b}+3)-\ell_c(\ell_c+1)} & \text{otherwise.} \end{cases}$$

Note that is it necessary to pay attention when integrating CC equations close to $r=s$, that is when the electron coordinate r and the dipolar charge separation s have the same magnitude, as the potential (4) is not differentiable therein.

In the external region $[r_m : +\infty]$, the basis wave functions are denoted $u_{b;c_b}^+(r)$. By construction, at very large distances of the order of hundreds of a_0 (asymptotic region), $u_{b;c_b}^+(r) \neq 0$ for $c_b = (j_{c_b}, \ell_{c_b})$ and $u_{b;c}^+(r) = 0$ for other channels $c \neq c_b$. The asymptotic behavior of external channel functions is discussed in Sec. IV B below.

Both sets of internal and external basis functions are used to expand the channel function $u_c(r)$:

$$u_c(r) = \begin{cases} \sum_b C_b^0 u_{b;c}^0(r) & \text{for } r \leq r_m, \\ \sum_b C_b^+ u_{b;c}^+(r) & \text{for } r \geq r_m \end{cases} \qquad (18)$$

The matching conditions at $r = r_m$

$$\sum_b \left[C_b^0 u_{b;c}^0(r_m) - C_b^+ u_{b;c}^+(r_m) \right] = 0, \qquad (19)$$

$$\sum_b \left[C_b^0 \frac{du_{b;c}^0}{dr}(r_m) - C_b^+ \frac{du_{b;c}^+}{dr}(r_m) \right] = 0, \qquad (20)$$

form a linear system of equations: $AX = 0$. The condition of $\det A = 0$ determines the energy of a bound or resonant state. (One can thus see that $\det A$ is thus the generalization of the Jost function for CC equations.) Once

the eigenenergy has been found, the amplitudes C_b^0, C_b^+ are given by the eigenvector X of A. The overall norm is determined by the condition:

$$\sum_c \int_0^{+\infty} |u_c(r)|^2 \, dr = 1. \tag{21}$$

B. The coupled-channel equations in the asymptotic region

At large distances, $V_{cc'}(r)$ can be written as:

$$V_{cc'}(r) = \frac{\hbar^2}{2m_e} \left[\frac{\chi_{cc'}}{r^2} + V_3(r) \right], \tag{22}$$

where $\chi_{cc'}$ is a constant and $V_3(r)$ decreases for $r \to +\infty$ as r^{-3}. In the following, we shall assume that $V_3(r) = 0$ in the asymptotic region. As the numerical integration up to $r \sim 100 \, a_0$ is stable, the error made by neglecting V_3 is around $10^{-6} \, a_0^{-3}$, which is sufficiently small to insure that the asymptotic zone has been practically reached.

Let us first consider the case of an infinite moment of inertia $I \to +\infty$. Here, Eq. (13) becomes:

$$u_c''(r) = \frac{\ell_c(\ell_c + 1)}{r^2} u_c(r) + \sum_{c'} \frac{\chi_{cc'}}{r^2} u_{c'}(r) - k^2 u_c(r), \tag{23}$$

where $k = \sqrt{E}$. The outgoing solution of (23) in a basis channel b can be written in terms of spherical Hankel functions:

$$u_{b;c}^+(r) = g_c^{(b)} H_{\ell_{eff}^{(b)}}^+ (kr), \tag{24}$$

where $\ell_{eff}^{(b)}$ is an effective angular momentum given by eigenvalues of the eigenproblem

$$\ell_c(\ell_c + 1) g_c^{(b)} + \sum_{c'} \chi_{cc'} g_{c'}^{(b)} = \ell_{eff}^{(b)}(\ell_{eff}^{(b)} + 1) g_c^{(b)}. \tag{25}$$

Indeed, it immediately follows from Eqs. (23) and (25) that:

$$u_{b;c}^+(r)'' = \left(\frac{\ell_{eff}^{(b)}(\ell_{eff}^{(b)} + 1)}{r^2} - k^2 \right) u_{b;c}^+(r), \tag{26}$$

so the physical interpretation of $\ell_{eff}^{(b)}$ in terms of an effective angular momentum is justified.

If I is finite, however, solutions of Eq. (13) are no longer analytical at large distances. Nevertheless, it is possible to construct an adiabatic approximation for $u_c(r)$ in the asymptotic region. To this end, one defines the linear momentum $k_c = \sqrt{E - j_c(j_c + 1)/I}$ for a channel c. In the asymptotic region, Eq. (13) becomes:

$$u_c''(r) = \frac{\ell_c(\ell_c + 1)}{r^2} u_c(r) + \sum_{c'} \frac{\chi_{cc'}}{r^2} u_{c'}(r) - k_c^2 u_c(r), \tag{27}$$

where, compared to Eq. (23), k is replaced by the channel momentum k_c. This approximation can be applied if $|E| \gg j_c(j_c + 1)/I$ for all channels of importance. In those cases, one can introduce an ansatz for $u_c(r)$ by replacing k by k_c in Eq. (24). The relative error on a basis function $u_+^{(b;c)}(r)$ associated with this approximation is

$$\sum_{c'} \left| \frac{\chi_{cc'}}{r^2} \frac{g_{c'}^{(b)}}{g_c^{(b)}} \left(\frac{H_{\ell_{eff}^{(b)}}^+ (k_{c'}r)}{H_{\ell_{eff}^{(b)}}^+ (k_c r)} - 1 \right) \right|, \tag{28}$$

i.e., is of the order of $|k_c - k_{c'}|/r^2$.

In practical calculations, $I \sim 10^5$ and $j_{max} \sim 7$. This gives $j_{max}(j_{max} + 1)/I \sim 10^{-4}$. Consequently, if $|E| > 10^{-3}$ Ry, the error $|k_c - k_{c'}|/r^2 < 10^{-6} \, a_0^{-3}$ for $r \sim 100 \, a_0$ is close to that associated with the neglect of $V_3(r)$. On can thus see that the proposed ansatz accounts for the coupling term (22) in many cases. However, this approximation breaks down for weakly-bound/unbound states with $|E| < 10^{-4}$ Ry; hence, a more adequate theoretical method based on a resonant state expansion needs to be introduced.

V. DIAGONALIZATION WITH THE BERGGREN BASIS

Another way to find eigenstates of the CC problem (13) is to diagonalize the associated Hamiltonian in a complete basis of single-particle states. Since our goal is to describe weakly-bound or unbound states, special care should be taken to treat the asymptotic part of wave functions as precisely as possible. A suitable basis for this problem is the one-body Berggren ensemble [49, 65, 85]. This basis is generated by a finite-depth spherical potential and contains bound (b), decaying (d), and scattering (s) one-body states. Fot that reason, the Berggren ensemble is ideally suited to deal with structures having large spatial extensions (such as halos or Rydberg states) or outgoing behavior (such as decaying resonances). Some recent applications, in a many-body context, have been reviewed in Ref. [54].

A. The Berggren basis

The finite-depth potential generating the Berggren ensemble can be chosen arbitrarily. To improve the convergence, however, it is convenient in practical applications to use a one-body potential, which is as close as possible to the Hartree-Fock field of the Hamiltonian in question. Therefore, in the case of the one-body problem (13), the most optimal potential to generate the Berggren basis is the diagonal part of $v_{cc'}(r)$. This means that the basis states $\Phi_{k,c}(r)$ are eigenstates of the spherical potential $v_{cc}(r)$:

$$\Phi_{k,c}''(r) = \left(\frac{\ell_c(\ell_c + 1)}{r^2} + v_{cc}(r) - k^2 \right) \Phi_{k,c}(r) \tag{29}$$

that obey the following boundary conditions:

$$\Phi_{k,c}(r) \sim C^0 r^{\ell_c+1}, \ r \sim 0 \ \text{for all states,} \tag{30}$$

$$\Phi_{k,c}(r) \sim C^+ H^+_{\ell_c}(kr), \ r \to +\infty \ (b,d), \tag{31}$$

$$\Phi_{k,c}(r) \sim C^+ H^+_{\ell_c}(kr) + C^- H^-_{\ell_c}(kr), \ r \to +\infty \ (s), \tag{32}$$

where the boundary conditions at $r \sim 0$ and at $r \to +\infty$ for scattering states (s) are standard, and for bound and decaying states (b,d) one imposes the outgoing boundary condition. This condition reduces to the standard decaying boundary condition for bound states, as $H^+_{\ell_c}(kr) \to 0$ when $r \to +\infty$ in this case. Note that k in Eq. (29) is in general complex.

The scattering states are normalized to the Dirac delta, which results in a condition for the C^- and C^+ amplitudes in (32) [49]:

$$\langle \Phi_{k,c} | \Phi_{k',c} \rangle = \delta(k - k') \Leftrightarrow 2\pi C^+ C^- = 1. \tag{33}$$

The normalization of bound states is standard as well, but that of decaying resonant states is not. Indeed, resonant states rapidly oscillate and diverge exponentially in modulus along the real r-axis; hence, one cannot calculate their norm in the same way as for the bound states.

The solution of this problem is provided by the exterior complex scaling [86], i.e., one calculates the norm of the resonant state using complex r radii:

$$\langle \Phi_{k,c} | \Phi_{k,c} \rangle = \int_0^R \Phi^2_{k,c}(r) \, dr$$
$$+ \int_0^{+\infty} \Phi^2_{k,c}(R + xe^{i\theta}) \, e^{i\theta} \, dx,, \tag{34}$$

where R is a radius taken sufficiently large so that condition (31) is fulfilled. In the above formula, θ is an angle of rotation chosen so that $\Phi_{k,c}(R + xe^{i\theta}) \to 0$ for $x \to +\infty$, which is always possible provided θ is larger than a critical value depending on k [87]. Note that no modulus enters Eq. (34). This arises from the finite-lifetime character of resonant states, which requires us to use the biorthogonal scalar product [54, 87–90]. It can be shown [88–90] that the norm defined in Eq. (34) is indeed independent of R and θ, as expected from a norm. Since the expression (34) is also valid for bound states, bound and decaying states enter the Berggren ensemble as one family of resonant states.

The exterior complex scaling can be used to calculate matrix elements of a one-body operator $O(r)$ as well, provided it decreases faster than $1/r$ along the complex r-contour:

$$\langle \Phi_{k',c'} | O | \Phi_{k,c} \rangle = \int_0^R \Phi_{k',c'}(r) \, O_{cc'}(r) \, \Phi_{k,c}(r) \, dr$$
$$+ \int_0^{+\infty} \Phi_{k',c'}(z(x)) \, O_{cc'}(z(x)) \, \Phi_{k,c}(z(x)) \, e^{i\theta} \, dx, \tag{35}$$

where $z(x) = R + xe^{i\theta}$, and $|\Phi_{k,c}\rangle$ and $|\Phi_{k',c'}\rangle$ can here be bound, decaying, or scattering states.
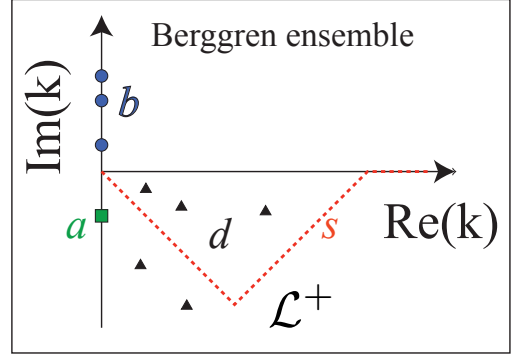
B. The Berggren completeness relation

FIG. 1. (Color online) Berggren ensemble in the complex momentum plane. The bound (b) and antibound (a) states are distributed along the imaginary k-axis at $Im(k) > 0$ and $Im(k) < 0$, respectively. The decaying resonant states (d) are located in the fourth quadrant $(Re(k) > 0, Im(k) < 0)$. The Berggren completeness relation involves bound states, scattering states (s) on the $\mathcal{L}^+$ contour, and decaying states lying between the real-k axis and $\mathcal{L}^+$. If antibound states are included, the $\mathcal{L}^+$ contour has to be slightly deformed [54, 91]. If the contour $\mathcal{L}^+$ lies on the real k-axis, the Berggren completeness relation reduces to the Newton completeness relation [54, 92] involving bound and real-energy scattering states.

Figure 1 shows a distribution the Berggren ensemble in the complex momentum plane. To determine the basis, one first chooses a $\mathcal{L}^+$ contour in the fourth quadrant containing the decaying eigenstates. The scattering states of the ensemble lie on this contour. The resonant part of the ensemble contains the bound states lying on the imaginary-k axis and those decaying states of (29) that are found in the region between the real-k axis and $\mathcal{L}^+$. The Berggren basis is built from all those states:

$$\sum_{n \in (b,d)} |\Phi_{k_n,c}\rangle \langle \Phi_{k_n,c}| + \int_{\mathcal{L}^+} |\Phi_{k,c}\rangle \langle \Phi_{k,c}| \ dk = 1. \tag{36}$$

This completeness relation corresponds to a given channel c; hence, one has to construct Berggren ensembles for all the channels considered in Eq. (13).

In order to be able to use (36) in practice, one needs to discretize $\mathcal{L}^+$. Our method of choice is to apply the Gauss-Legendre quadrature to each of the segments defining $\mathcal{L}^+$ in Fig. 1. The last segment, chosen along the real-k axis, extends to the large cutoff momentum $k = k_{max}$ that is sufficiently large to guarantee completeness to desired precision. It is then convenient to renormalize scattering states using the corresponding Gauss-Legendre weights ω_{k_n}:

$$|\Phi_{n,c}\rangle = \sqrt{\omega_{k_n}} \, |\Phi_{k_n,c}\rangle. \tag{37}$$

The discretized Berggren completeness relation, used in

practical computations, reads:

$$\sum_{i=1}^{N} |\Phi_{i,c}\rangle \langle \Phi_{i,c}| \simeq 1, \qquad (38)$$

where the N basis states $|\Phi_{i,c}\rangle$ include all bound, decaying, and discretized scattering states of the channel c. By using Eq. (37), the Dirac delta normalization of scattering states has been replaced by the usual normalization to Kronecker's delta. in this way, all $|\Phi_{i,c}\rangle$ states can be treated on the same footing in Eq. (38), as in any basis of discrete states.

C. Hamiltonian matrix in the Berggren basis

As the basis states $|\Phi_{i,c}\rangle$ are generated by $v_{cc}(r)$, the Hamiltonian matrix within the same channel c is diagonal:

$$\langle \Phi_{i',c}|h|\Phi_{i,c}\rangle = \left(k_i^2 + \frac{j_c(j_c+1)}{I} \right) \delta_{ii'} \qquad (39)$$

Matrix elements between two basis states belonging to different channels c and c' are:

$$\langle \Phi_{i',c'}|h|\Phi_{i,c}\rangle = \langle \Phi_{i',c}|v|\Phi_{i,c}\rangle$$
$$= \int_0^R \Phi_{i',c'}(r) \, v_{cc'}(r) \, \Phi_{i,c}(r) \, dr$$
$$+ \int_0^{+\infty} \Phi_{i',c'}(z(x)) \, v_{cc'}(z(x)) \, \Phi_{i,c}(z(x)) \, e^{i\theta} \, dx, \quad (40)$$

where the complex scaling (35) can be used, because $v_{cc'}(r)$ decreases at least as fast as r^{-2}.

As the off-diagonal matrix elements are present only for $c \neq c'$, the Berggren basis generated by Eq. (29) is optimal. The channel wave functions $u_c(r)$ can be expressed in the Berggren basis by diagonalizing the matrix of h (39,40).

VI. CALCULATION PARAMETERS

Results of the direct integration method (DIM) depend both on the parameters of the pseudo-potential (3) and on the cutoff value of the electron orbital angular momentum ℓ_{max} considered in the CC problem. They are fixed to reproduce the experimental value of the ground state energy of the LiCl$^-$ anion: $E_{exp} = -4.483 \cdot 10^{-2}$ Ry [29].

The most important term in (3) is the dipole potential V_μ, which depends only on the dipole moment μ and the size s of the neutral molecule. The remaining parameters of the pseudo-potential are taken from Ref. [24], namely: $\alpha_0 = 15.3 \, a_0^3$, $\alpha_2 = 1.1 \, a_0^3$, $r_0 = 2.2 \, a_0$, $r_c = 2.828 \, a_0$, $Q_{zz} = 3.28 \, e a_0^2$, and $V_0 = 2.0$ Ry. The moment of inertia parameters are: $I = 150,000 \, m_e a_0^2$ for LiCl$^-$, $240,000 \, m_e a_0^2$ for LiI$^-$, $82,000 \, m_e a_0^2$ for LiF$^-$,

and $26,000 \, m_e a_0^2$ for LiH$^-$. The dipole moment of each molecule considered in this work is known experimentally and has been taken from the NIST database.
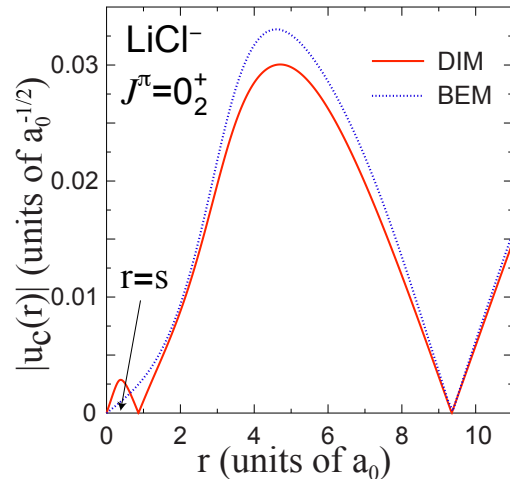

FIG. 2. (Color online) The modulus of the channel wave function $u_{j=0,\ell=0}$ near $r = 0$ for the first excited $J^\pi = 0_2^+$ state of LiCl$^-$ calculated in DIM (solid line) and BEM (dotted line) with $\ell_{max} = 9$. The charge separation s of LiCl has been adjusted in both approaches to the experimental ground state energy in the limit $\ell_{max} \to \infty$.

For $\ell_{max} = 9$ the ground state energy of the LiCl$^-$ anion is reproduced by taking the charge separation $s_{DIM}^{(9)} = 0.336 \, a_0$. To remove the dependence of results on ℓ_{max} in the DIM, the ground state energy of LiCl$^-$ is extrapolated for $\ell_{max} \to \infty$, and the size of the charge separation s is adjusted to reproduce the experimental binding energy. In this case, $s_{DIM}^{(\infty)} = 0.337 \, a_0$. The matching radius was taken as $r_m = a_0$. This value was found to optimize the DIM procedure.

Anion spectra in the BEM depend sensitively on the cutoff parameter k_{max} of the single-particle basis. However, as we shall see in Sec. VII, for a chosen value of k_{max} they are practically independent of ℓ_{max}. In this study, we have chosen $k_{max} = 1.53 \, a_0^{-1}$ for each partial wave in order to attain both a good numerical precision and approximately the same value of the dipole size parameter s as in DI. In this case, $s_{BEM}^{(9)} = s_{BEM}^{(\infty)} = 0.336 \, a_0$. We have used complex contours with straight segments connecting points: $k_1 = (0,0)$, $k_2 = (0.15, -i0.04)$, $k_3 = (1,0)$, and $k_4 = k_{max}$ in units of a_0^{-1}. Each scattering contour has been discretized with 220 points. The precise form of the contour does not change results; since the applications carried out in this work pertain to bound states only, we could have used real scattering contours, i.e., the Newton completeness relation [54, 92].

VII. NUMERICAL TESTS AND BENCHMARKING

Along with the asymptotic behavior of channel wave functions, treated approximately with the DIM and exactly within BEM, the Hamiltonian (2) cannot be identically represented in both approaches. Indeed, since the potential $V_\mu(r)$ (4) is not differentiable at $r = s$, it cannot be treated exactly in BEM because the channel wave functions expanded in the Berggren basis are analytic by construction. In practice, this translates into a node beyond $r = s$ in DIM channel wave functions, which is absent in BEM. This is illustrated in Fig. 2 for a
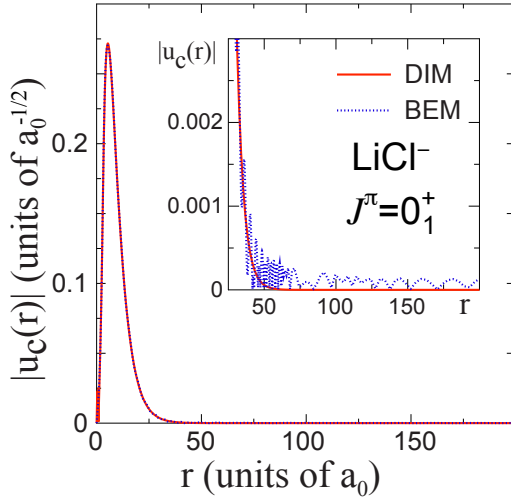

FIG. 3. (Color online) The modulus of the channel wave function $u_{j=0, \ell=0}$ for the $J^\pi = 0_1^+$ ground state of LiCl$^-$ calculated in DIM (solid line) and BEM (dotted line) with $\ell_{max} = 9$. At large distances, spurious wiggles appear in BEM results (see the inset) due to basis truncation.

$(j = 0, \ell = 0)$ channel function corresponding to the first excited $J^\pi = 0_2^+$ state of LiCl$^-$. It is to be noted, however, that beyond this point the channel wave functions calculated with both methods are very close and – as will be discussed later – this near-origin pathology has a very small impact on the total energy as the contribution from this region is small.

As discussed in Sec. IV B, DIM is inadequate for states with very small energies, while BEM has been shown to be very precise in this case. On the other hand, for states with binding energies typically greater than 10^{-2} Ry, BEM yields channel wave functions that exhibit spurious low-amplitude oscillations. Figure 3 illustrates such wiggles in the tail of the channel wave function $u_{j=0, \ell=0}$ of the $J^\pi = 0_1^+$ ground state of LiCl$^-$. For such well-bound states that quickly decay with r, the standard size of the Berggren basis (measured in terms of contour discretization points and k_{max}) is not sufficient. The DIM is thus preferable for such cases, as the asymptotic behavior of well-bound states is treated almost exactly (see Sec. IV B).

The direct integration becomes numerically unstable when the channel orbital angular momentum becomes large, around $\ell_c = 10$, even for the states with relatively large binding energies. In this case, the matrix of basis channel wave functions $u_{b;c}^0(r_m)$ and $u_{b;c}^+(r_m)$ and their derivatives, introduced in Sec. IV A in the context of matching conditions at $r = r_m$, is ill-conditioned and its eigenvector of zero eigenvalue becomes imprecise. This results in a discontinuity at r_m and spurious occupation of channels with large orbital angular momentum $\ell_c > 10$. This is illustrated in Fig. 4 for the $J^\pi = 0_1^+$ ground state of LiCl$^-$. A a result, the energy and spatial extension of the electron cloud distribution of the CC eigenstate become incorrect.
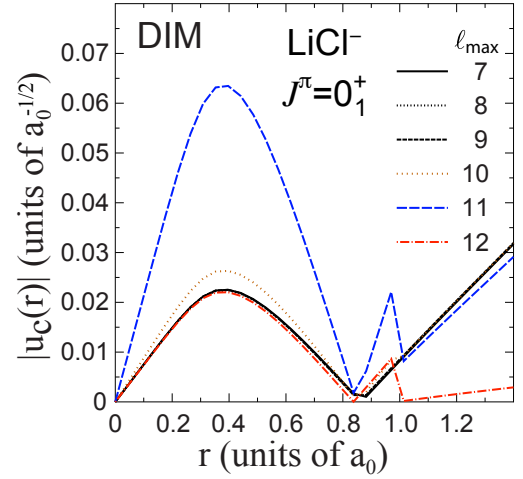

FIG. 4. (Color online) The modulus of the channel wave function $u_{j=0, \ell=0}$ for the $J^\pi = 0_1^+$ ground state of LiCl$^-$ calculated in DIM with several values of ℓ_{max}. For $\ell_{max} \geq 10$, one may notice the development of a discontinuity at the matching point $r_m = a_0$. In such cases, the channel wave function becomes ill-conditioned, introducing serious errors in CC eigenenergy and eigenfunction.

The convergence of the LiCl$^-$ ground state energy with respect to ℓ_{max} is shown in Fig. 5. One may notice an exponential convergence of calculated DIM energies with ℓ_{max} for $6 \leq \ell_{max} \leq 10$ and a clear deviation for $\ell \geq 11$, which is related to the discontinuity of channel wave functions for $\ell_c > 10$. The energy calculated in BEM is perfectly stable with ℓ_{max}.

The rapid converge of BEM with ℓ is due to k_{max}-truncation of the single-particle basis that suppresses contributions from large-ℓ configurations. This is illustrated in Fig. 6, which displays the average modulus of the off-diagonal matrix element of the channel-channel coupling in BEM:

$$A_{c,c'} = \frac{1}{N^2} \sum_{n,n'}^{N} |\langle \Phi_{n',c'} | V | \Phi_{n,c} \rangle| \qquad (41)$$

between the first channel $c = (j = 0, \ell = 0)$ and higher-ℓ channels c'. Only the channels with $\ell_c \leq 5$ and
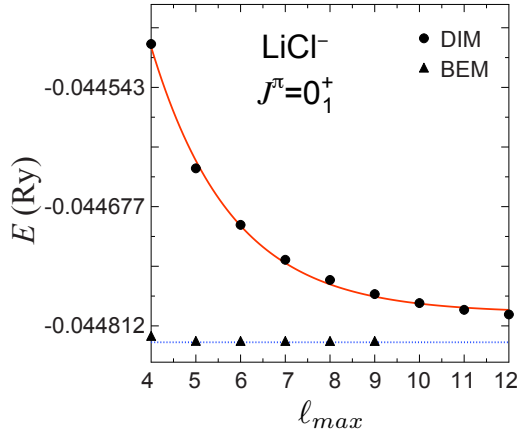
FIG. 5. (Color online) The dependence of the LiCl$^-$ ground state energy on ℓ_{max} in DIM (dots) and BEM (triangles). The DIM results converge exponentially (red line). This allows us to determine the asymptotic value of energy at $\ell_{max} \to \infty$.

FIG. 7. (Color online) The dependence of the LiCl$^-$ ground state r.m.s. radius on ℓ_{max} DIM (dots) and BEM (dotted line). The DIM results are stable up to $\ell_{max} = 10$.
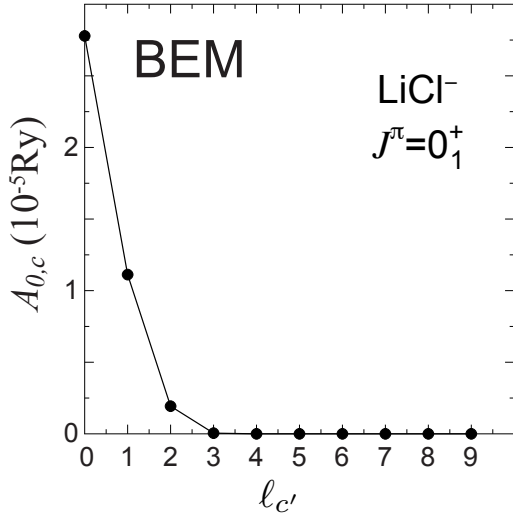

FIG. 6. Average off-diagonal matrix element $A_{0,c}$ (41) of the channel-channel coupling in BEM between the channel ($j = 0, \ell = 0$) and c' for the $J^\pi = 0_1^+$ ground state of LiCl$^-$.

FIG. 8. (Color online) Most important channel wave functions $u_c(r)$ with $c = (j, \ell)$ for the $J^\pi = 0_1^+$ ground state of LiCl$^-$, as calculated in DIM (solid line) and BEM (dashed line) with $\ell_{max} = 9$.

$|\ell_c - \ell_{c'}| \leq 3$ contribute significantly to the channel coupling matrix element. We checked that this is generally the case. Using the same truncation, the DIM yields numerically stable results. In this case, the energies of well-bound states ($|E| > 10^{-2}$ Ry) agree in both methods.

The numerical instability of DIM at large ℓ_{max} leads to a collapse of calculated radii. Figure 7 shows the dependence of the ground state r.m.s. radius of LiCl$^-$ on ℓ_{max}. This result, together with discussion of Fig. 6, suggests that the BEM can provide practical guidance on the minimal number of channels in the CC approach.

In practical applications, spurious oscillations in BEM channel wave functions for well-bound states can be taken care of by extrapolating wave functions from the inter-
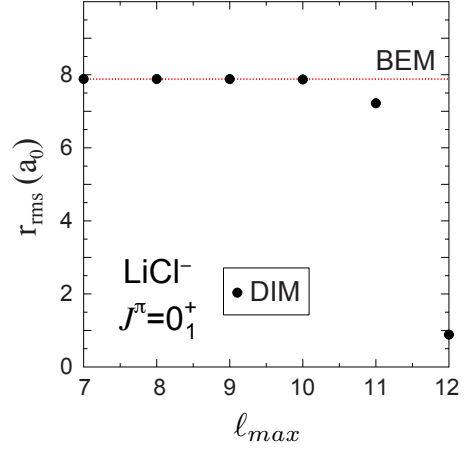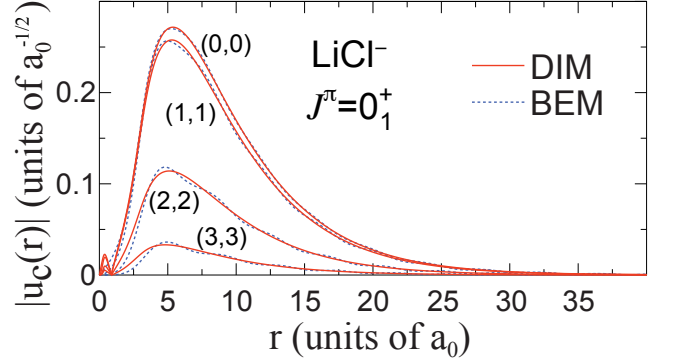
mediate region of r, where they are reliably calculated, into the asymptotic region. This can be done by applying the analytical expression:

$$\tilde{u}_c(r) \equiv \lim_{r \gg 0} u_c(r) = e^{ik_c r} \sum_{j=1}^{M} \frac{\alpha_j^{(c)}}{r^j}, \qquad (42)$$

where k_c is the channel momentum and $\alpha_j^{(c)}$ are parameters to be determined by the fit. The precision of this procedure can be assessed by computing the norm of the eigenstate. Using this procedure, one obtains perfectly stable r.m.s. radii in BEM for different values of ℓ_{max}, as can be seen in Fig. 7.

Figures 8-10 compare the four most important channel wave functions (ℓ, j) of DIM and BEM corresponding to the three lowest $J_i^\pi = 0_1^+$ eigenstates of LiCl$^-$. For the ground state, both approaches predict the same energy $E = -4.483 \cdot 10^{-2}$ Ry and the channel functions are practically identical. For the first excited state, the
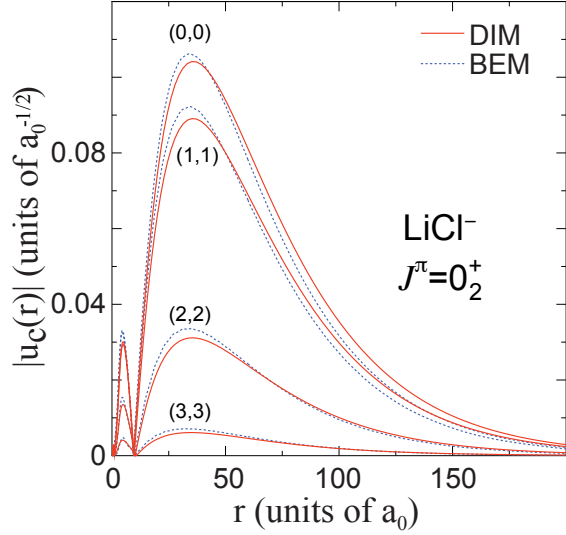
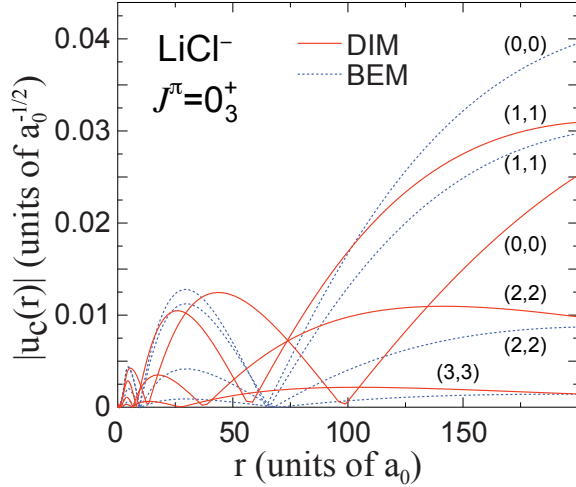FIG. 9. (Color online) Similar to Fig. 8 but for the first excited $J^\pi = 0_2^+$ state of LiCl$^-$.

FIG. 10. (Color online) Similar to Fig. 8 but for the second excited $J^\pi = 0_3^+$ state of LiCl$^-$.

agreement is still reasonable. Here, the energy in DIM is $E = -7.374 \cdot 10^{-4}$ Ry while BEM gives slightly more binding: $E = -8.241 \cdot 10^{-4}$ Ry. Consequently, the BEM wave functions decay faster than those computed with DIM. For a second excited 0_3^+ state, both methods differ markedly. This state has a sub-threshold nature, with $E_{DIM} = -7.051 \cdot 10^{-6}$ Ry and $E_{BEM} = -9.907 \cdot 10^{-6}$ Ry. For this extremely diffused state, the direct integration method fails completely. This is manifested by the very different nodal structure of channel wave functions in DIM seen in Fig. 10.

A stringent test of the computational framework to describe dipolar molecules is provided by the analytic result $\mu_{cr} = 0.639\,ea_0$ for the fixed dipole ($I \to \infty$) [42]. To this end, we performed BEM calculations for a dipolar system

at steadily decreasing moments of inertia [20, 21]. For each value of I, the dipolar anion energies have been calculated for 1080 values of μ in the interval $0.6 \le \mu \le 3.0$. Only 170 energies satisfying the subthreshold condition $E < E_{lim} = -10^{-8}$ Ry were retained to minimize the numerical error. These energies correspond to an interval $\Delta\mu \simeq 0.377$ of the dipole moment. We checked, that in this energy interval, μ_{cr} can be obtained by using the expression

$$E(\mu) = (\mu + b)^{\frac{a}{\mu}} e^c \qquad (43)$$

to extrapolate the calculated energy down to $E = 0$. One should stress however, that an excellent energy fit in the subthreshold region does not guarantee an excellent estimate of the critical dipole moment. The values of μ_{cr} extracted by this extrapolation procedure can be considered reliable only if $\Delta\mu$, which depends on the chosen precision E_{lim}, is close to the critical dipole moment. In the cases studied, this criterion is approximately satisfied only for the ground state and the first excited 0^+ state. The critical dipole moments for these states in anions with the dipole length $s = 4a_0$ are shown in Table I for various moments of inertia. The agreement with the ana-

TABLE I. Critical dipole moments for dipolar anions in the two lowest 0^+ states calculated in this work (BEM) and in Ref. [21] for the charge separation $s = 4a_0$ and different moments of inertia I. The analytic result at $I \to \infty$ [41, 42] is $\mu_{cr} = 0.639\,ea_0$.

$I(m_e a_0^2)$	$\mu_{cr}^{(0)}\,(ea_0)$		$\mu_{cr}^{(1)}\,(ea_0)$	
	BEM	Ref. [21]	BEM	Ref. [21]
10^4	0.937	0.843	1.024	1.515
10^6	0.674	0.750	0.633	1.145
10^8	0.639	0.715	0.622	0.974
10^{10}	0.639	—	0.622	—
10^{15}	0.639	—	0.62	—

lytic limit is excellent for the ground state configuration, and is fairly good for the first excited 0^+ state. This is very encouraging, considering the slow convergence with I and various sources of numerical errors in the $E \to 0$ regime [20].

VIII. RESULTS FOR SPECTRA AND RADII OF DIPOLAR ANIONS

Energies and r.m.s. radii of the lowest bound 0^+ and 1^- states of LiI$^-$, LiCl$^-$, LiF$^-$, and LiH$^-$ dipolar anions predicted in this study are listed in Table II.

One can see that for each total angular momentum J^π there are at most three bound eigenstates in each system. The r.m.s. radius of an electron cloud shows a spectacular increase with decreasing the binding energy of the state. For the subthreshold states, such as 0_3^+ and 1_3^-, the radius is of the order of hundreds to thousands a_0.

TABLE II. Energies and r.m.s. radii for 0^+ and 1^- bound states of selected dipolar anions obtained in DIM ($\ell_{max} = 9$) and BEM. The parameters of the calculation are given in Sec. VI. The numbers in parentheses denote powers of 10.

Anion	state	E (Ry)		r_{rms} (a_0)	
		DIM	BEM	DIM	BEM
LiI$^-$	0_1^+	-5.079(-2)	-5.023(-2)	7.569(0)	7.620(0)
	0_2^+	-9.374(-4)	-1.037(-3)	5.112(1)	4.759(1)
	0_3^+	-1.502(-5)	-1.797(-5)	3.719(2)	3.308(2)
	1_1^-	-5.079(-2)	-4.995(-2)	7.569(0)	7.641(0)
	1_2^-	-9.291(-4)	-1.023(-3)	5.112(1)	4.886(1)
	1_3^-	-1.261(-7)	-1.099(-5)	3.423(3)	3.464(2)
LiCl$^-$	0_1^+	-4.483(-2)	-4.483(-2)	7.885(0)	7.894(0)
	0_2^+	-7.374(-4)	-8.241(-4)	5.632(1)	5.017(1)
	0_3^+	-7.051(-6)	-9.907(-6)	5.124(2)	4.106(2)
	1_1^-	-4.482(-2)	-4.458(-2)	7.885(0)	7.915(0)
	1_2^-	-7.241(-4)	-8.067(-4)	5.633(1)	5.337(1)
	1_3^-	-3.062(-7)	-8.159(-7)	2.066(3)	8.831(2)
LiF$^-$	0_1^+	-2.795(-2)	-2.983(-2)	9.117(0)	8.991(0)
	0_2^+	-3.022(-4)	-3.525(-4)	8.098(1)	7.501(1)
	0_3^+	—	-6.101(-8)	—	3.363(3)
	1_1^-	-2.793(-2)	-2.968(-2)	9.117(0)	9.010(0)
	1_2^-	-2.782(-4)	-3.277(-4)	8.124(1)	7.520(1)
LiH$^-$	0_1^+	-2.149(-2)	-2.370(-2)	1.011(1)	9.698(0)
	0_2^+	-1.491(-4)	-1.922(-4)	1.058(2)	9.297(1)
	1_1^-	-2.142(-2)	-2.353(-2)	1.011(1)	9.717(0)
	1_2^-	-7.942(-5)	-1.231(-4)	1.146(2)	9.591(1)

TABLE III. Energies for 0^+ bound states of selected dipolar anions obtained in DIM in this work ($\ell_{max} = 9$) and in Ref. [24]. The numbers in parentheses denote powers of 10.

Anion	state	E (Ry)	
		This work	Ref. [24]
LiI$^-$	0_1^+	-5.079(-2)	-4.998(-2)
	0_2^+	-9.374(-4)	-1.022(-3)
	0_3^+	-1.502(-5)	-1.999(-5)
LiCl$^-$	0_1^+	-4.483(-2)	-4.483(-2)
	0_2^+	-7.374(-4)	-7.497(-4)
	0_3^+	-7.051(-6)	-9.775(-6)
LiF$^-$	0_1^+	-2.795(-2)	-2.793(-2)
	0_2^+	-3.022(-4)	-3.366(-4)
	0_3^+	—	-8.746(-7)
LiH$^-$	0_1^+	-2.149(-2)	-2.352(-2)
	0_2^+	-1.491(-4)	-1.926(-4)

can be traced back to the cutoff value of the electron orbital angular momentum when solving CC equations. In Ref. [24], adopted ℓ_{max} was small, typically $\ell_{max} = 4$ [37], whereas it is fairly large, $\ell_{max} = 9$, in our work. As seen in Fig. 5 and discussed in Sec. VII, energies of weakly-bound states obtained in DIM do converge slowly with ℓ_{max}. Therefore, calculations employing low ℓ_{max} values cannot be useful when performing extrapolation $\ell_{max} \to \infty$.

TABLE IV. Dipole moments of selected dipolar anions adopted in this work and in Ref. [24].

Anion	μ (ea_0)	
	This work	Ref. [24]
LiI$^-$	2.911384272	2.911384272
LiCl$^-$	2.805158089	2.793355179
LiF$^-$	2.472316049	2.478610934
LiH$^-$	2.313370205	2.321238811

Energy spectra and radii of dipolar anions do not change significantly in the limit $\ell_{max} \to \infty$. Usually, the extrapolated results for both E and r_{rms} agree very well with those in Table II ($\ell_{max} = 9$). For instance, the extrapolated values for the 1_2^+ state in LiH$^-$ are $E = -7.931 \cdot 10^{-5}$ Ry and $r_{rms} = 1.147 \cdot 10^2 \, a_0$.

The DIM and BEM results are generally consistent for both energy and radii though significant quantitative differences persist for excited, weakly-bound states of anions where the DIM is not expected to work. In the case of LiF$^-$, the BEM predicts the existence of the third 0_3^+ state at an energy $-6.1 \cdot 10^{-8}$ Ry, which is absent in DIM.

It is instructive to compare our DIM results with those found in Ref. [24] using a similar approach. Table III lists energies of the lowest 0^+ bound states of LiI$^-$, LiCl$^-$, LiF$^-$, and LiH$^-$ dipolar anions obtained in both studies, and Table IV shows the adopted values of dipole moments.

The two calculations agree reasonably well for the lowest-lying states; some difference stems from slightly different dipole moments used in Ref. [24] and here. Indeed, while the charge separation in both studies was adjusted to reproduce the experimental ground state energy of LiCl$^-$, the fitted values of s in both calculations are different: $s = 0.3335 \, a_0$ in Ref. [24] and $s_{DIM} = 0.336 \, a_0$ here.

The largest deviations, seen for weakly-bound states,

IX. CONCLUSIONS

In this study, we applied the theoretical open-system framework based on the Berggren ensemble to a problem of weakly-bound states of dipole-bound anions. The method has been benchmarked by using the traditional technique of direct integration of CC equations. While a fairly good agreement between the two methods has been found for well-bound states, the direct integration technique breaks down for weakly-bound states with energies $|E| < 10^{-4}$ Ry, which is comparable with the rotational energy of the anion. For those subthreshold configurations, the Berggren expansion is an obvious tool of choice.

The inherent problem of the DIM is the lack of stability of results when the number of channels is increased. Indeed, the method breaks down when the channel or-

bital angular momentum becomes large; around $\ell_c = 10$. This can be traced back to the applied matching condition. We demonstrated that this pathology is absent in BEM. Here, the rapid converge with ℓ is guaranteed by an effective softening of the interaction through the momentum cutoff k_{max}, which suppresses contributions from high-ℓ partial waves.

The future applications of BEM will include the structure of quadrupole-bound anions [43, 93–95] and the continuum structure of anions, including the characterization of low-lying resonances. In the latter case, the BEM will provide a viable alternative to the computational method based on the non direct product discrete-variable representation [96], which was applied for resonant scattering in dipole-dipole collisions [97], stripping and excitations in p+He$^+$ collisions [98], and breakup of weakly-bound halo nuclei [99].

[1] K. Riisager, D. V. Fedorov, and A. S. Jensen, Europhys. Lett. **49**, 547 (2000).
[2] V. Rotival, K. Bennaceur, and T. Duguet, Phys. Rev. C **79**, 054309 (2009).
[3] P. G. Hansen and B. Jonson, Europhys. Lett. **4**, 409 (1987).
[4] I. Tanihata, J. Phys. G **22**, 157 (1996).
[5] A. Cobis, A. S. Jensen, and D. V. Fedorov, J. Phys. G **23**, 401 (1997).
[6] A. S. Jensen, K. Riisager, D. V. Fedorov, and E. Garrido, Rev. Mod. Phys. **76**, 215 (2004).
[7] I. Mazumdar, A. R. P. Rau, and V. S. Bhasin, Phys. Rev. Lett. **97**, 062503 (2006).
[8] T. K. Lim, S. K. Duffy, and W. C. Damer, Phys. Rev. Lett. **38**, 341 (1977).
[9] N. Moiseyev and C. Corcoran, Phys. Rev. A **20**, 814 (1979).
[10] R. E. Grisenti, W. Schöllkopf, J. P. Toennies, G. C. Hegerfeldt, T. Köhler, and M. Stoll, Phys. Rev. Lett. **85**, 2284 (2000).
[11] D. Bressanini, G. Morosi, L. Bartini, and M. Mella, Few-Body Syst. **31**, 199 (2002).
[12] Y. Li, Q. Gou, and T. Shi, Phys. Rev. A **74**, 032502 (2006).
[13] R. Lefebvre, O. Atabek, M. Šindelka, and N. Moiseyev, Phys. Rev. Lett. **103**, 123003 (2009).
[14] S. I. Vinitsky, L. I. Ponomarev, I. V. Puzynin, T. P. Puzynina, L. N. Somov, and M. P. Faifman, Sov. Phys. JETP **52**, 353 (1980).
[15] A. D. Gocheva, V. V. Gusev, V. S. Melezhik, L. I. Ponomarev, I. V. Puzynin, T. P. Puzynina, L. N. Somov, and S. I. Vinitsky, Phys. Lett. B **153**, 349 (1985).
[16] J. Mitroy, Phys. Rev. Lett. **94**, 033402 (2005).
[17] K. Varga, J. Mitroy, J. Z. Mezei, and A. T. Kruppa, Phys. Rev. A **77**, 044502 (2008).
[18] F. Ferlaino and R. Grimm, Physics **3**, 9 (2010).
[19] W. R. Garrett, Chem. Phys. Lett. **5**, 393 (1970).
[20] W. R. Garrett, Phys. Rev. A **3**, 961 (1971).
[21] W. R. Garrett, J. Chem. Phys. **73**, 5721 (1980).
[22] W. R. Garrett, Phys. Rev. A **22**, 1769 (1980).
[23] W. R. Garrett, Phys. Rev. A **23**, 1737 (1981).
[24] W. R. Garrett, J. Chem. Phys. **77**, 3666 (1982).
[25] L.G. Christophorou, *Atomic and Molecular Radiation Physics*, Wiley, New York (1971).
[26] R.N. Compton, P.W. Reinhardt, and C.D. Cooper, J. Chem. Phys. **66**, 3305 (1977).
[27] S. F. Wong and G. J. Schulz, Phys. Rev. Lett. **33**, 134 (1974).
[28] K. Rohr and F. Linder, J. Phys. B **9**, 2521 (1976).
[29] J. Carlsten, J. Peterson, and W. Lineberger, Chem. Phys. Lett. **37**, 5 (1976).
[30] K. D. Jordan and W. Luken, J. Chem. Phys. **64**, 2760 (1976).
[31] K. R. Lykke, R. D. Mead, and W. C. Lineberger, Phys. Rev. Lett. **52**, 2221 (1984).
[32] E. A. Brinkman, S. Berger, J. Marks, and J. I. Brauman, J. Chem. Phys. **99**, 7586 (1993).
[33] A. S. Mullin, K. K. Murray, C. P. Schulz, and W. C. Lineberger, J. Phys. Chem. **97**, 10281 (1993).
[34] C. Desfrançois, H. Abdoul-Carime, and J. P. Schermann, Int. J. Mol. Phys. B **10**, 1339 (1996).
[35] J. R. Smith, J. B. Kim, and W. C. Lineberger, Phys. Rev. A **55**, 2036 (1997).
[36] H. Abdoul-Carime and C. Desfrançois, Eur. Phys. J. D **2**, 149 (1998).
[37] S. Ard, W. R. Garrett, R. N. Compton, L. Adamowicz, and S. G. Stepanian, Chem. Phys. Lett. **473**, 223 (2009).
[38] R. N. Compton and N. I. Hammer, *Advances in Gas Phase Ion Chemistry*, vol. 4 (Elsevier, Amsterdam, 2001).
[39] K. D. Jordan and F. Wang, Annu. Rev. Phys. Chem. **54**, 367 (2003).
[40] V. E. Chernov, A. V. Danilyan, and B. A. Zon, Phys. Rev. A **80**, 022702 (2009).
[41] E. Fermi and E. Teller, Phys. Rev. **72**, 399 (1947).
[42] J.-M. Lévy-Leblond, Phys. Rev. **153**, 1 (1967).
[43] W. R. Garrett, J. Chem. Phys. **128**, 194309 (2008).
[44] J. Kalcher and A. F. Sax, J. Mol. Struct. (Theochem) **498**, 77 (2000).
[45] J. Kalcher and A. F. Sax, Chem. Phys. Lett. **326**, 80 (2000).
[46] P. Skurski, I. Dabkowska, A. Sawicka, and J. Rak, Chem. Phys. **279**, 101 (2002).
[47] H. Estrada and W. Domcke, J. Phys. B **17**, 279 (1984).
[48] H. R. Sadeghpour, J. L. Bohn, M. J. Cavagnero, B. D. Esry, I. I. Fabrikant, J. H. Macek, and A. R. P. Rau, J. Phys. B **33**, R93 (2000).
[49] T. Berggren, Nucl. Phys. A **109**, 265 (1968).

[50] N. Michel, W. Nazarewicz, M. Płoszajczak, and K. Bennaceur, Phys. Rev. Lett. **89**, 042502 (2002).

[51] N. Michel, W. Nazarewicz, M. Płoszajczak, and J. Okołowicz, Phys. Rev. C **67**, 054311 (2003).

[52] N. Michel, W. Nazarewicz, M. Płoszajczak, Phys. Rev. C, **70** 064313 (2004).

[53] R. Id Betan, R. J. Liotta, N. Sandulescu, and T. Vertse, Phys. Rev. Lett. **89**, 042501 (2002).

[54] N. Michel, W. Nazarewicz, M. Płoszajczak, and T. Vertse, J. Phys. G **36**, 013101 (2009).

[55] G. Gamow, Z. Phys. **51**, 204 (1928).

[56] I. M. Gel'fand and N. Ya. Vilenkin, *Generalized functions*, Vol. 4 , Academic Press , New-York (1961).

[57] K. Maurin, *Generalized Eigenfunction expansions and unitary representations of topological groups*, Polish Scientific Publishers, Warsaw (1968).

[58] A. Bohm, *The rigged Hilbert space and quantum mechanics*, Lecture Notes in Physics 78, Springer, New York (1978).

[59] R. de la Madrid, Eur. J. Phys. **26**, 287 (2005).

[60] R. de la Madrid, J. Math. Phys. **53**, 102113 (2012).

[61] A.F.J. Siegert, Phys. Rev. **56**, 750 (1939).

[62] R.E. Peierls, Proc. R. Soc. (London) **A 253**, 16 (1959).

[63] J. Humblet and L. Rosenfeld, Nucl. Phys. **26**, 529 (1961).

[64] B. Gyarmati and A. T. Kruppa, Phys. Rev. A **33**, 2989 (1986).

[65] P. Lind, Phys. Rev. C **47**, 1903 (1993).

[66] C.G. Bollini, O. Civitarese, A.L. De Paoli, and M.C. Rocca, Phys. Lett. **B 382**, 205 (1996).

[67] R. de la Madrid, and M. Gadella, Am. J. Phys. **70**, 626 (2002).

[68] E. L. Hamilton and C. H. Greene, Phys. Rev. Lett. **89**, 263003 (2002).

[69] E. Kapuścik, and P. Szczeszek, Czech. J. Phys. **53**, 1053 (2003).

[70] E. Hernandez, A. Járegui, and A. Mondragon, Phys. Rev. A **67**, 022721 (2003).

[71] E. Kapuścik, and P. Szczeszek, Found. Phys. Lett. **18**, 573 (2005).

[72] R. Santra, J. M. Shainline, and C. H. Greene, Phys. Rev. A **71**, 032703 (2005).

[73] J. Julve, and F.J. de Urries, quant-ph/0701213.

[74] R. de la Madrid, quant-ph/0607168.

[75] K. Toyota, O. I. Tolstikhin, T. Morishita, and S. Watanabe, Phys. Rev. A **76**, 043418 (2007).

[76] A. T. Kruppa, B. Barmore, W. Nazarewicz, and T. Vertse, Phys. Rev. Lett. **84**, 4549 (2000).

[77] B. Barmore, A. T. Kruppa, W. Nazarewicz, and T. Vertse, Phys. Rev. C **62**, 054315 (2000).

[78] A. T. Kruppa and W. Nazarewicz, Phys. Rev. C **69**, 054311 (2004).

[79] O. I. Tolstikhin, Phys. Rev. A **73**, 062705 (2006).

[80] O. I. Tolstikhin, Phys. Rev. A **77**, 032712 (2008), URL `http://link.aps.org/doi/10.1103/PhysRevA.77.032712`.

[81] W. R. Garrett, J. Chem. Phys. **133**, 224103 (2010).

[82] W. R. Garrett, J. Chem. Phys. **69**, 2621 (1978).

[83] W. R. Garrett, J. Chem. Phys. **71**, 651 (1979).

[84] I. J. Thompson, Comput. Phys. Rep. **7**, 167 (1988).

[85] T. Berggren and P. Lind, Phys. Rev. C **47**, 768 (1993).

[86] B. Gyarmati and T. Vertse, Nucl. Phys. A **160**, 523 (1971).

[87] N. Michel, W. Nazarewicz, M. Płoszajczak, and J. Okołowicz, Phys. Rev. C **67**, 054311 (2003).

[88] J. Aguilar and J.M. Combes, Commun. Math. Phys. **22**, 269 (1971).

[89] E. Balslev, J.M. Combes, Commun. Math. Phys. **22**, 280 (1971).

[90] B. Simon, Commun. Math. Phys. **27**, 1 (1972).

[91] N. Michel, W. Nazarewicz, M. Płoszajczak, and J. Rotureau, Phys. Rev. C **74**, 054305 (2006).

[92] R. Newton, *Scattering Theory of Waves and Particles* (Springer-Verlag, New York Heidelberg Berlin, 1982).

[93] A. Ferron, P. Serra, and S. Kais, J. Chem. Phys. **120**, 18 (2004).

[94] C. Desfrançois, Y. Bouteiller, J. P. Schermann, D. Radisic, S. T. Stokes, K. H. Bowen, N. I. Hammer, and R. N. Compton, Phys. Rev. Lett. **92**, 083003 (2004).

[95] W. R. Garrett, J. Chem. Phys. **136**, 054116 (2012).

[96] V. S. Melezhik, AIP Conference Proc. **1479**, 1200 (2012).

[97] V. S. Melezhik and C.-Y. Hu, Phys. Rev. Lett. **90**, 083202 (2003).

[98] V. S. Melezhik, J. S. Cohen, and C.-Y. Hu, Phys. Rev. A **69**, 032709 (2004).

[99] P. Capel, D. Baye, and V. S. Melezhik, Phys. Rev. C **68**, 014612 (2003).